Journal of Nuclear Materials 381 (2008) 129–136

Contents lists available at ScienceDirect

Journal of Nuclear Materials

journal homepage: www.elsevier.com/locate/jnucmat

Constitutive material model for the prediction of stresses in irradiated anisotropic graphite components

Derek K.L. Tsang *, Barry J. Marsden

Nuclear Graphite Research Group, School of Mechanical, Aerospace and Civil Engineering, The University of Manchester, P.O. Box 88, Manchester M60 1QD, UK

A B S T R A C T

As well as acting as a moderator and reflector, graphite is used as a structural component in many gas-cooled fission nuclear reactors. Therefore the ability to predict the structural integrity of the many graphite components which make up a graphite reactor core is important in safety case assessments and reactor core life prediction. This involves the prediction of the service life stresses in the individual graphite components. In this paper a material model for the prediction of stresses in anisotropic graphite is presented. The time-integrated non-linear irradiated graphite material model can be used for stress analysis of graphite components subject to both fast neutron irradiation and radiolytic oxidation. As an example a simple stress analysis of a typical reactor graphite component is presented along with a series of sensitivity studies aimed at investigating the importance of the various material property changes involved in graphite component stress prediction.

1. Introduction

Cores of graphite moderated reactors are constructed from many thousand graphite components. Throughout reactor life it is important that the graphite core structure remains sufficiently strong and undistorted to permit adequate cooling as well as accommodating loading and unloading of nuclear fuels and the necessary movements of control rods. Hence the ability to predicted stresses in graphite components is important in safety case assessments and reactor core life predictions. In the early reactors these components were manufactured from highly anisotropic graphite such as the Pile Grade A (PGA) graphite used in the early UK Magnox reactors. Later, the reactor cores were constructed from more uniform semi-isotropic graphite. However, in most cases the anisotropic nature of the graphite should be taken account of when predicting component service stresses. This paper presents a constitutive model for the prediction of stresses in irradiated anisotropic graphite components subject to fast neutron damage and radiolytic oxidation, along with an example of its use. To illustrate the use of the model, a simple graphite brick manufactured from PGA graphite is analysed. The constitutive material equations for irradiated PGA graphite are first developed. Then a three-dimensional model is used to predict stresses in a typical PGA graphite brick subject to fast neutron irradiation and radiolytic oxidation, followed by a series of sensitivity studies on material properties.

Pile Grade A graphite was produced from a particular petroleum needle-coke which was a by product from oil refining. Coal tar pitch was used as the binder. PGA consists of about 80% coke and 20% binder. The extrusion process used in the manufacture of PGA graphite tended to align the petroleum-coke particles parallel to the direction of extrusion which results in a highly-orientated structure. Thus, the graphite crystallographic layer planes tend to lie parallel to the block extrusion axis, thus producing a product having strongly transversely anisotropic properties, i.e. properties measured parallel to the extrusion direction differ from that perpendicular to it, in some case by a factor of ~2.

Fast neutron irradiation leads to significant component dimension and materials property change, including changes to Young's modulus, coefficient of thermal expansion (CTE) and thermal conductivity. In addition when irradiated under load graphite components exhibit significant irradiation creep. In a carbon-dioxide cooled graphite moderated reactor radiolytic oxidation leads to significant graphite weight loss. Radiolytic weight loss occurs fairly uniformly within a graphite component and may amount to greater than 20% weight loss throughout the life of a reactor. This weight loss further modifies the modulus strength and thermal conductivity of graphite. Furthermore graphite weight loss is thought to modify the irradiation creep and dimensional change rate. All of these property changes must be accounted for in a constitutive model for irradiated graphite. Typical unirradiated material properties of the PGA used in this analysis are given in Table 1.

Internal stresses are induced in graphite components mainly due to the non-uniform dimension change distribution caused by fast neutron fluence and temperature gradients across a typical

* Corresponding author.
E-mail address: kwong-lai.tsang@manchester.ac.uk (D.K.L. Tsang).

0022-3115/$ - see front matter © 2008 Elsevier B.V. All rights reserved.
doi:10.1016/j.jnucmat.2008.07.025

Table 1
Unirradiated material data for PGA graphite

Material properties	Unirradiated material properties
Young's modulus	$E_0^{\parallel} = 11.27$ GPa $E_0^{\perp} = 6.21$ GPa
Poisson's ratio	$\nu^{\parallel} = 0.05, \quad \nu^{\perp} = 0.12$
Creep modulus	$E_{0,C}^{\parallel} = 11.27$ GPa $E_{0,C}^{\perp} = 6.21$ GPa
Creep Poisson ratio	$\nu_C^{\parallel} = 0.05, \ \nu_C^{\perp} = 0.12$
CTE	$\alpha_{(20-120)}^{\parallel} = 0.9 \times 10^{-6}/^{\circ}\mathrm{C}$ $\alpha_{(20-120)}^{\perp} = 2.8 \times 10^{-6}/^{\circ}\mathrm{C}$

graphite component. Fortunately, irradiation creep relaxes these self-induced stresses to some extent.

In a previous study [1] an irradiation material model for isotropic nuclear graphite was developed and implemented into the ABAQUS [2] finite element code. In this paper a material model for PGA graphite is considered. Both models are capable of predicting stresses in graphite components subject to fast neutron irradiation and radiolytic oxidation, although the models can be applied to any isotropic or anisotropic graphite component irradiated in a carbon-dioxide coolant or in an inert atmosphere.

2. Anisotropic irradiated graphite material model

A comprehensive irradiated material property database is required for any graphite component stress analysis. The data required includes irradiated elastic material properties, irradiation creep properties, irradiation induced dimensional changes and changes to the coefficient of thermal expansion. These properties are required as a function of fast neutron fluence, irradiation temperature and radiolytic weight loss. Empirical irradiated material property data trends are derived from the analysis of data obtained by irradiating small samples in a material test reactor (MTR). Typical irradiated PGA material property data can be found in [3]. The units for the irradiation fluence and irradiation temperature are usually expressed in terms of equivalent DIDO nickel dose $\times 10^{20}$ n/cm^2 (EDND) and equivalent DIDO temperature °C (EDT), respectively.

2.1. Irradiated elastic material data

It is assumed that the irradiated elastic modulus E in perpendicular ($\perp$) and parallel ($\parallel$) directions and shear modulus G in parallel direction can be calculated by a multiplication rule as

$$\begin{aligned} E^{\perp} &= E_0^{\perp} \cdot S^{\perp}(\gamma, T) \cdot W(\phi), \\ E^{\parallel} &= E_0^{\parallel} \cdot S^{\parallel}(\gamma, T) \cdot W(\phi), \\ G^{\parallel} &= G_0^{\parallel} \cdot S^{\parallel}(\gamma, T) \cdot W(\phi), \end{aligned} \tag{1}$$

where γ, T and ϕ are irradiation fluence, temperature and weight loss fraction respectively, $E_0^{\perp}$ and $E_0^{\parallel}$ are the unirradiated Young's modulus in perpendicular and parallel directions, respectively. $G_0^{\parallel}$ is the unirradiated shear modulus in parallel direction. The functions $S^{\perp}$ and $S^{\parallel}$ are fractional modulus changes due to irradiation fluence and temperature. The function $W(\phi)$ is a weight loss decay term usually defined as $W = \exp(-4.8\phi)$. In this analysis it is assumed that Poisson's ratio in both the perpendicular and parallel directions remain constant under irradiation.

It is assumed that elastic modulus changes due to fast neutron irradiation by two separated mechanisms: pinning of dislocations within the graphite crystallites by irradiation induced lattice defects and structural changes to the polycrystalline microstructure arising from large irradiation induced dimensional changes of the crystallites. The fractional change factors $S^{\perp}$ and $S^{\parallel}$ are the product of both the pinning term and structure term. Fig. 1 shows the fractional change factors for PGA graphite in both material directions.

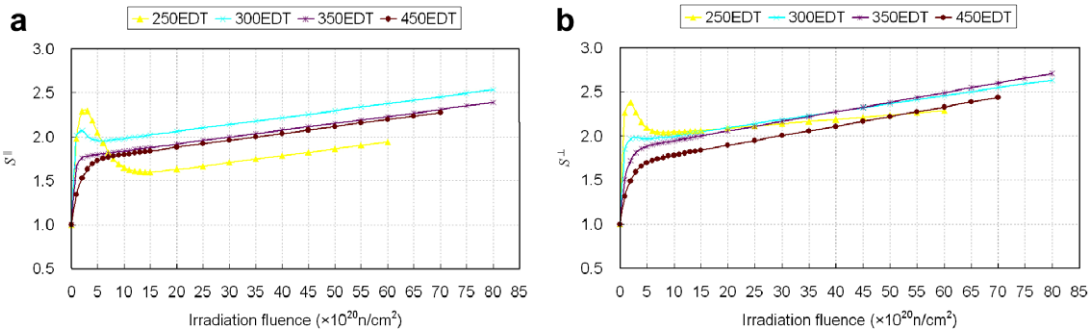

Fig. 1. Fractional change factors in the parallel (a) and perpendicular (b) directions at various temperatures.

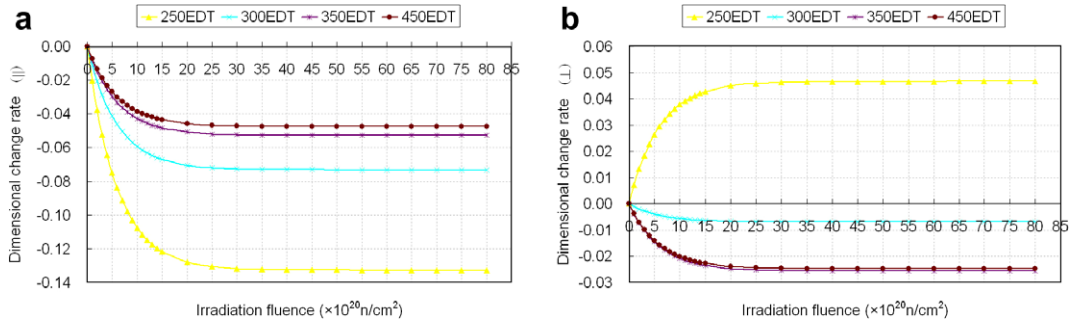

Fig. 2. Dimensional change rate in the parallel (a) and perpendicular (b) directions at various temperatures.

2.2. Irradiation creep material data

It is assumed that the creep moduli can be calculated as

$$E_C^{\perp} = \frac{E_{0,C}^{\perp} \cdot S^{\perp}(\gamma,T) \cdot W(\phi) \cdot f}{P},$$
$$E_C^{\parallel} = \frac{E_{0,C}^{\parallel} \cdot S^{\parallel}(\gamma,T) \cdot W(\phi) \cdot f}{P}, \quad (2)$$
$$G_C^{\parallel} = \frac{G_{0,C}^{\parallel} \cdot S^{\parallel}(\gamma,T) \cdot W(\phi) \cdot f}{P},$$

where f is the ratio of unirradiated static to dynamic Young's modulus and P is a non-temperature dependent pinning term. $E_{0,C}^{\perp}$, $E_{0,C}^{\parallel}$ and $G_{0,C}^{\parallel}$ are the unirradiated creep moduli. It is usually assumed that the unirradiated creep moduli are same as unirradiated elastic moduli. Also same fractional changes factor as in elastic moduli have been applied on creep moduli. Since the parameters f and P are constants, the creep modulus can be written in term of elastic modulus as

$$E_C^{\perp} = \beta E^{\perp},$$
$$E_C^{\parallel} = \beta E^{\parallel}, \quad (3)$$
$$G_C^{\parallel} = \beta G^{\parallel},$$

where β is a constant.

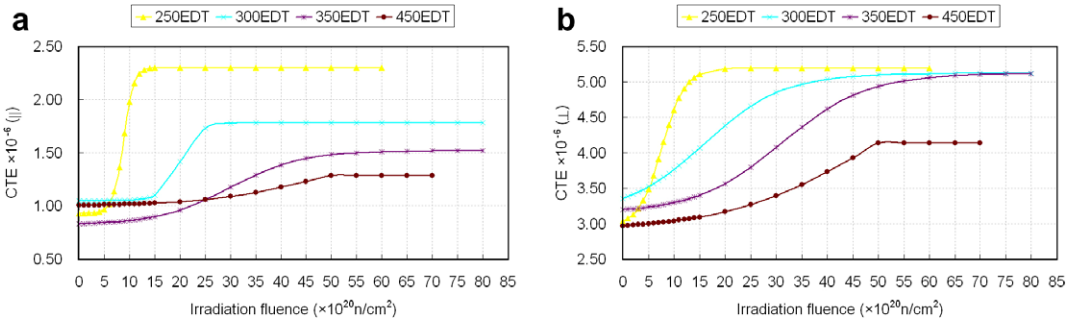

Fig. 3. CTE in the parallel (a) and perpendicular (b) directions at various temperatures.

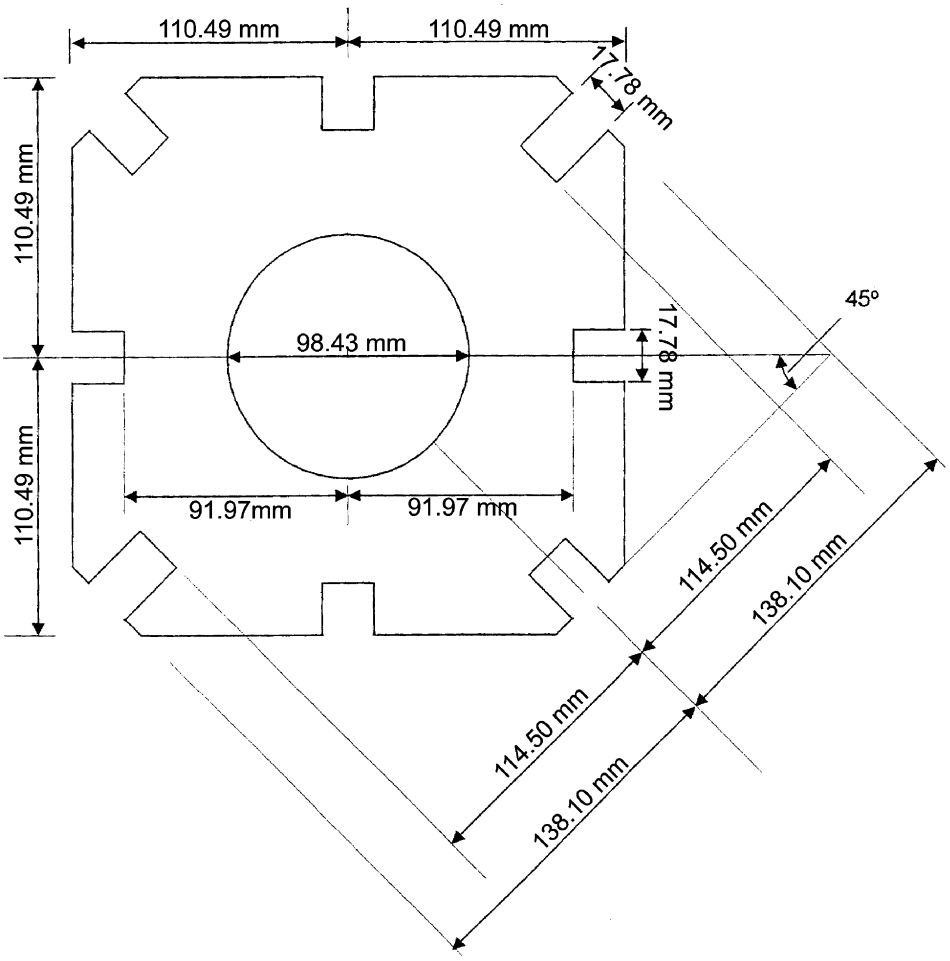

Fig. 4. Cross-sectional dimension of an octagonal nuclear graphite brick.

2.3. Dimensional changes

The dimensional change is a function of irradiation fluence and temperature. Typical profiles of dimensional change rate in parallel and perpendicular for PGA graphite are shown in Fig. 2. It is assumed that the radiolytic oxidation has negligible effect on dimensional change. For PGA irradiated in this temperature range it is assumed that dimensional change 'turn around' is not reached and therefore the dimensional change rate eventually reaches a constant value, see Fig. 2. When this point is reached the driving force for increasing stress is constant and the stress peaks, thereafter being reduced by irradiation creep.

2.4. CTE

The irradiated CTE $\bar{\alpha}_{(20-120)}$ data measured over the range 20–120 °C is taken from [3] and is given as a function of EDT and fluence. However, the typical reactor gas operating temperatures are in the range 235–375 °C. Therefore the instantaneous CTE value α_i is adjusted accordingly using an expression reported in [4]:

$$\alpha_i = \bar{\alpha}_{(20-120)} + B(T), \tag{4}$$

where $B(T)$ is the adjustment due to different temperature range:

$$B(T) = -2.66343 \times 10^{-1} + 4.03616 \times 10^{-3}T + 1.67126 \times 10^{-7}T^2 - 3.37798 \times 10^{-9}T^3 + 1.57676 \times 10^{-12}T^4. \tag{5}$$

Also it is assumed that the radiolytic oxidation has negligible effect on CTE. Fig. 3 show the irradiated CTE for PGA graphite in both material directions.

3. Constitutive equations

As in our previous study [1], the constitutive equation has been implemented into ABAQUS finite element code via user material subroutine. The change in total strain within the PGA model is the sum of change of five different strain components:

$$\Delta\boldsymbol{\varepsilon}^{\text{total}} = \Delta\boldsymbol{\varepsilon}^{\text{e}} + \Delta\boldsymbol{\varepsilon}^{\text{th}} + \Delta\boldsymbol{\varepsilon}^{\text{dc}} + \Delta\boldsymbol{\varepsilon}^{\text{pc}} + \Delta\boldsymbol{\varepsilon}^{\text{sc}}, \tag{6}$$

where $\Delta\boldsymbol{\varepsilon}^{\text{th}}$ is the change in thermal strain, $\Delta\boldsymbol{\varepsilon}^{\text{dc}}$ is the change in dimensional change strain induced by irradiation, $\Delta\boldsymbol{\varepsilon}^{\text{pc}}$ is the change in primary creep strain and $\Delta\boldsymbol{\varepsilon}^{\text{sc}}$ is the change in secondary creep strain. Brief description about these strains will be given below, further detail based on isotropic properties is given in [1].

The elastic strain is related to the stress by means of the usual Hooke's law of linear elasticity, i.e.

$$\boldsymbol{\sigma} = \mathbf{D}\boldsymbol{\varepsilon}^{\text{e}}, \tag{7}$$

where the material matrix $\mathbf{D}$ is a function Young's modulus E and Poisson's ratio v. The incremental equation for the Hooke's law can be written as

$$\Delta\boldsymbol{\sigma} = \tilde{\mathbf{D}} \cdot \Delta\boldsymbol{\varepsilon}^{\text{e}} + \Delta\mathbf{D} \cdot \tilde{\boldsymbol{\varepsilon}}^{\text{e}}, \tag{8}$$

where tilde ($\sim$) represents the mean value in current increment.

The total creep strain can be expressed as sum of primary (transient) creep and secondary (steady state) creep, as in previous study [1]. Early creep experiments [5] for PGA under constant stress up to irradiation fluence 60×10^{21} n/cm^2 showed an initial transient creep strain equivalent to the corresponding elastic strain of unirradiated graphite. Also the creep experiments indicated the linear steady state creep rates and these rates in different orientation to be inversely proportional to the appropriate unirradiated Young's modulus. These experimental observations led to a model for total creep strain:

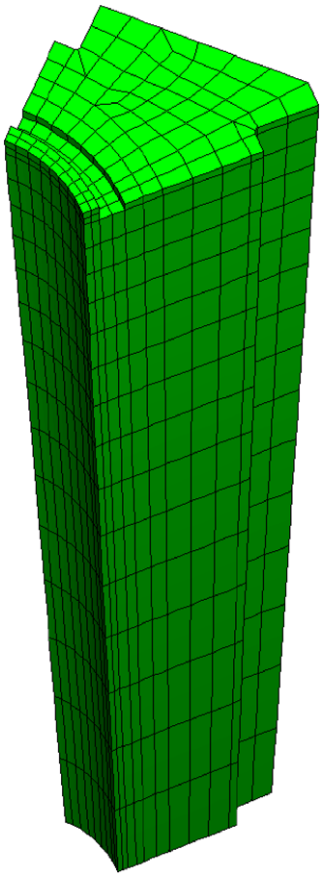

Fig. 5. Three-dimensional finite element mesh for the octagonal nuclear graphite brick.

$$\boldsymbol{\varepsilon}^{\text{creep}} = \boldsymbol{\varepsilon}^{\text{pc}} + \boldsymbol{\varepsilon}^{\text{sc}}, \tag{9}$$

$$\boldsymbol{\varepsilon}^{\text{pc}} = 4\text{e}^{-4\gamma} \int_0^{\gamma} \mathbf{D}_{\text{c}}\boldsymbol{\sigma}\text{e}^{4\gamma'}\text{d}\gamma', \tag{10}$$

$$\boldsymbol{\varepsilon}^{\text{sc}} = 0.23 \int_0^{\gamma} \mathbf{D}_{\text{c}}\boldsymbol{\sigma}\text{d}\gamma', \tag{11}$$

where $\boldsymbol{\varepsilon}^{\text{pc}}$ is primary creep, $\boldsymbol{\varepsilon}^{\text{pc}}$ is the secondary creep, $\mathbf{D}_{\text{c}}$ is creep material matrix which is a function of creep modulus E_{c} and creep Poisson's ratio v_{c}, and $\boldsymbol{\sigma}$ is the stress.

The primary creep equation in (10) is rewritten as a differential equation:

$$\frac{\text{d}\boldsymbol{\varepsilon}^{\text{pc}}}{\text{d}\gamma} = 4(\mathbf{D}_{\text{c}}\boldsymbol{\sigma} - \boldsymbol{\varepsilon}^{\text{pc}}) \tag{12}$$

and then incremental equation for primary creep can be written as

$$\Delta\boldsymbol{\varepsilon}^{\text{pc}} \approx 4(\tilde{\mathbf{D}}_{\text{c}}\tilde{\boldsymbol{\sigma}} - \tilde{\boldsymbol{\varepsilon}}^{\text{pc}})\Delta\gamma. \tag{13}$$

The incremental equation for secondary creep can be written as

$$\Delta\boldsymbol{\varepsilon}^{\text{sc}} = 0.23\tilde{\mathbf{D}}_{\text{c}}\tilde{\boldsymbol{\sigma}}\Delta\gamma. \tag{14}$$

The thermal strain can be written as

$$\boldsymbol{\varepsilon}^{\text{th}} = \boldsymbol{\alpha}_{(T_{\text{ref}}-T)}(T - T_{\text{ref}}), \tag{15}$$

where $\boldsymbol{\alpha}_{(T_{\text{ref}}-T)}$ is the mean CTE. Differentiating the above equation, we have

$$\Delta\boldsymbol{\varepsilon}^{\text{th}} = \Delta\boldsymbol{\alpha}_{(20-120)}\,(T - T_{ref}) + \boldsymbol{\alpha}_i\Delta T. \tag{16}$$

The mean CTE $\boldsymbol{\alpha}_{(20-120)}$ can be estimated from [3] and hence the instantaneous CTE $\boldsymbol{\alpha}_i$ can be found by using Eq. (4). Once the values

of CTE in different directions are known, the incremental thermal strain can be calculated from Eq. (16).

The dimensional change rates with respect to fluence are shown in Fig. 2. The incremental form of dimensional change strain can be written as

$$\Delta\boldsymbol{\varepsilon}^{\mathrm{dc}} = \left(\frac{\mathrm{d}\boldsymbol{\varepsilon}^{\mathrm{dc}}}{\mathrm{d}\gamma}\right)\Delta\gamma. \tag{17}$$

4. Numerical technique

In this section, the implementation of the irradiated PGA material model will be described. It is assumed that the average value in an increment is approximately calculated by central difference method, i.e.

$$\tilde{\boldsymbol{\sigma}} = \boldsymbol{\sigma}_i + \frac{\Delta\boldsymbol{\sigma}}{2}, \quad \tilde{\boldsymbol{\varepsilon}} = \boldsymbol{\varepsilon}_i + \frac{\Delta\boldsymbol{\varepsilon}}{2}. \tag{18}$$

Using Eq. (8), the primary creep and the secondary creep incremental equations can be written as

$$\Delta\boldsymbol{\varepsilon}^{\mathrm{pc}} - \frac{\Delta\gamma(2\tilde{\mathbf{D}}_{\mathrm{c}}\tilde{\mathbf{D}} + \tilde{\mathbf{D}}_{\mathrm{c}}\Delta\tilde{\mathbf{D}})}{1+2\Delta\gamma}\Delta\boldsymbol{\varepsilon}^{\mathrm{e}} = \frac{2\Delta\gamma\tilde{\mathbf{D}}_{\mathrm{c}}\Delta\tilde{\mathbf{D}}\boldsymbol{\varepsilon}_i^{\mathrm{e}} + 4\Delta\gamma(\tilde{\mathbf{D}}_{\mathrm{c}}\boldsymbol{\sigma}_i - \boldsymbol{\varepsilon}_i^{\mathrm{pc}})}{1+2\Delta\gamma}, \tag{19}$$

$$\Delta\boldsymbol{\varepsilon}^{\mathrm{sc}} - \zeta\Delta\gamma\left(\frac{2\tilde{\mathbf{D}}_{\mathrm{c}}\tilde{\mathbf{D}} + \tilde{\mathbf{D}}_{\mathrm{c}}\Delta\tilde{\mathbf{D}}}{4}\right)\Delta\boldsymbol{\varepsilon}^{\mathrm{e}} = \zeta\Delta\gamma\left(\tilde{\mathbf{D}}_{\mathrm{c}}\boldsymbol{\sigma}_i + \frac{\tilde{\mathbf{D}}_{\mathrm{c}}\Delta\tilde{\mathbf{D}}\boldsymbol{\varepsilon}_i^{\mathrm{pc}}}{2}\right), \tag{20}$$

where $\zeta = 0.23$. The total strain of Eq. (6) can be written as

$$\Delta\boldsymbol{\varepsilon}^{\mathrm{e}} + \Delta\boldsymbol{\varepsilon}^{\mathrm{pc}} + \Delta\boldsymbol{\varepsilon}^{\mathrm{sc}} = \Delta\boldsymbol{\varepsilon}^{\mathrm{total}} - \Delta\boldsymbol{\varepsilon}^{\mathrm{dc}} - \Delta\boldsymbol{\varepsilon}^{\mathrm{th}}. \tag{21}$$

The solution for $\Delta\boldsymbol{\varepsilon}^{\mathrm{e}}$ can be found by eliminating $\Delta\boldsymbol{\varepsilon}^{\mathrm{pc}}$ and $\Delta\boldsymbol{\varepsilon}^{\mathrm{sc}}$ in Eqs. (19) and (21):

$$\Delta\boldsymbol{\varepsilon}^{\mathrm{e}} = \left[\mathbf{I} + \Delta\gamma\left(\frac{1}{1+2\Delta\gamma} + \frac{\zeta}{4}\right)(2\tilde{\mathbf{D}}_{\mathrm{c}}\tilde{\mathbf{D}} + \tilde{\mathbf{D}}_{\mathrm{c}}\Delta\tilde{\mathbf{D}})\right]^{-1} \times \begin{bmatrix} \Delta\boldsymbol{\varepsilon}^{\mathrm{total}} - \Delta\boldsymbol{\varepsilon}^{\mathrm{dc}} - \Delta\boldsymbol{\varepsilon}^{\mathrm{th}} - \zeta\Delta\gamma\tilde{\mathbf{D}}_{\mathrm{c}}\boldsymbol{\sigma}_i \\ -\frac{4\ \Delta\gamma(\tilde{\mathbf{D}}_{\mathrm{c}}\boldsymbol{\sigma}_i - \boldsymbol{\varepsilon}_i^{\mathrm{pc}})}{1+2\ \Delta\gamma} \\ -\Delta\gamma(\frac{2}{1+2\Delta\gamma} + \frac{\zeta}{2})\tilde{\mathbf{D}}_{\mathrm{c}}\Delta\tilde{\mathbf{D}}\boldsymbol{\varepsilon}_i^{\mathrm{e}} \end{bmatrix}, \tag{22}$$

where $\mathbf{I}$ is an unit matrix. Once the solution for $\Delta\boldsymbol{\varepsilon}^{\mathrm{e}}$ is found, the solutions for $\Delta\boldsymbol{\varepsilon}^{\mathrm{pc}}$ and $\Delta\boldsymbol{\varepsilon}^{\mathrm{sc}}$ can be found by substituting $\Delta\boldsymbol{\varepsilon}^{\mathrm{e}}$ back into Eqs. (19) and (20).

The material Jacobian matrix required by the ABAQUS is a simple expression

$$\frac{\partial\Delta\boldsymbol{\sigma}}{\partial\Delta\boldsymbol{\varepsilon}^{\mathrm{e}}} = \tilde{\mathbf{D}}. \tag{23}$$

5. Application of the model

To perform stress analysis using finite element analysis for nuclear graphite under irradiation and radiolytic oxidation conditions, four different sets of input data are required. These are the

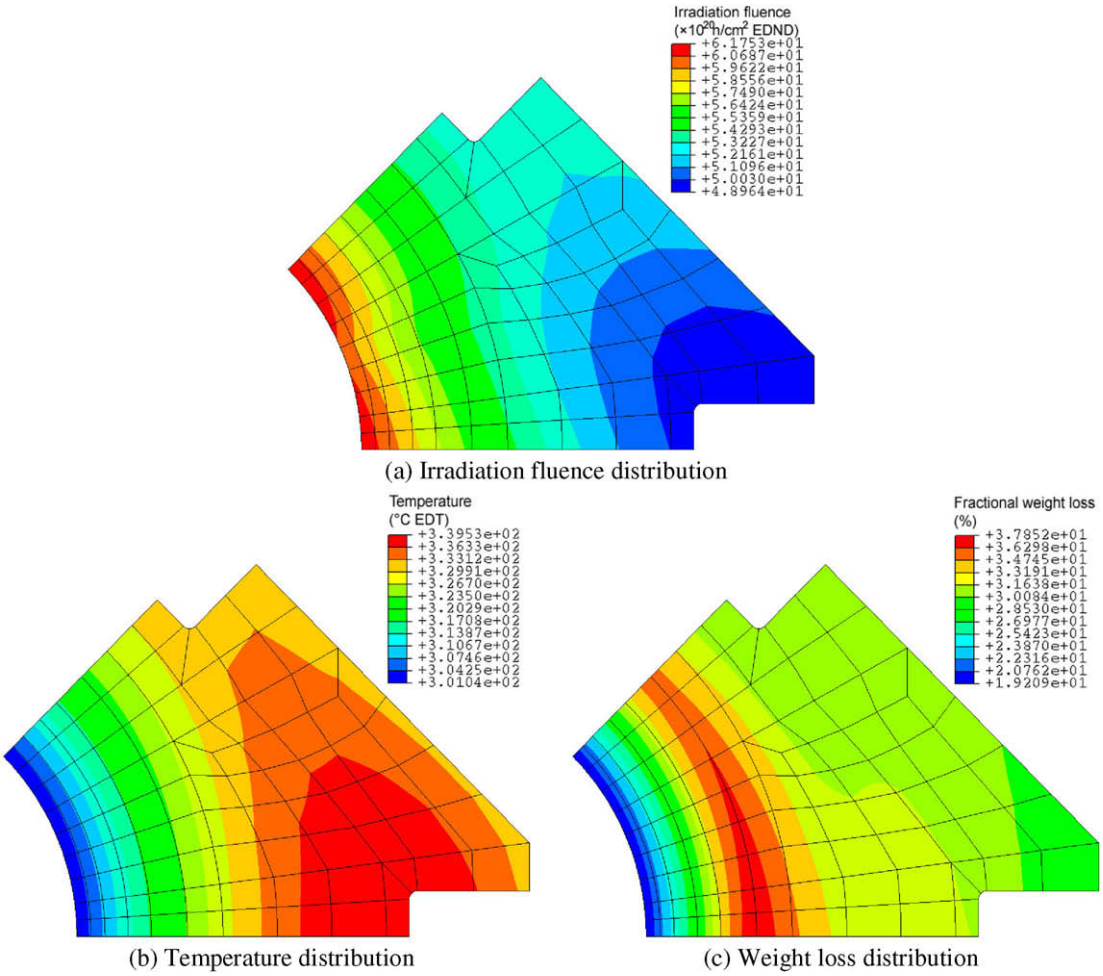

(a) Irradiation fluence distribution

(b) Temperature distribution

(c) Weight loss distribution

Fig. 6. Two-dimensional profiles of field variables at 30 FPY.

component geometry in the form of a finite element mesh, the reactor field variables data, and the unirradiated and irradiated graphite material properties data. The finite element mesh data includes the nodal coordinates and the finite element topology. The field variable data includes the time history of irradiation fluence, temperature and fractional weight loss at each nodal point. The graphite material properties data required are the coefficient of thermal expansion, the dimensional change, Young's and creep moduli, and elastic and creep Poisson's ratio.

The cross-sectional dimension of an octagonal brick is shown in Fig. 4. A three-dimensional finite element model for a full height octagonal brick is shown in Fig. 5. The maximum height of the finite element model is 822.96 mm. To reduce the size of the problem symmetry was taken advantage of and the finite element model represents only one-eight of the brick. In total there are 1664 hexahedra elements. The finite element model includes two keyways. In order to avoid stress singularity, the keyway corners have been modelled with a radius of 1.59 mm.

Three field variables required to perform the stress analysis were calculated using various analysis codes. Irradiation fluence within the brick is predicted using standard reactor physics codes by Monte Carlo simulation. The flux distribution is assumed to be constant through time. The temperature distribution is calculated using finite element method, incorporating nuclear heat generation, conduction, heat transfer at brick faces and convective heat transfer. The weight loss distribution is ether predicted by extrapolating reactor sampling data or if weight loss prediction is particularly complex using a specially written finite element code. The cross-sectional profiles of field variables at the end of 30 FPY are shown in Fig. 6.

For ease of presenting the results, only maximum hoop stress history and maximum axial stress history is presented. The results have been normalized by dividing by the peak hoop stress value (the magnitude of the others stress components are very small). A set of results for nominal PGA material model is shown in Fig. 7, and is designated as the baseline solution. Numerical results show that locations of maximum hoop stress and maximum axial stress are not the same and their location may change with time.

6. Sensitivity study

To investigate the influence of the various materials input data on stress prediction twelve cases have been studied. They are classified into four groups:

1. Elastic strain study.
2. Creep strain study.
3. Dimensional change study.
4. Thermal strain study.

There are at least two cases in each study (one for perpendicular and one for parallel). Each cases has been analysed for 30 full power years (FPY).

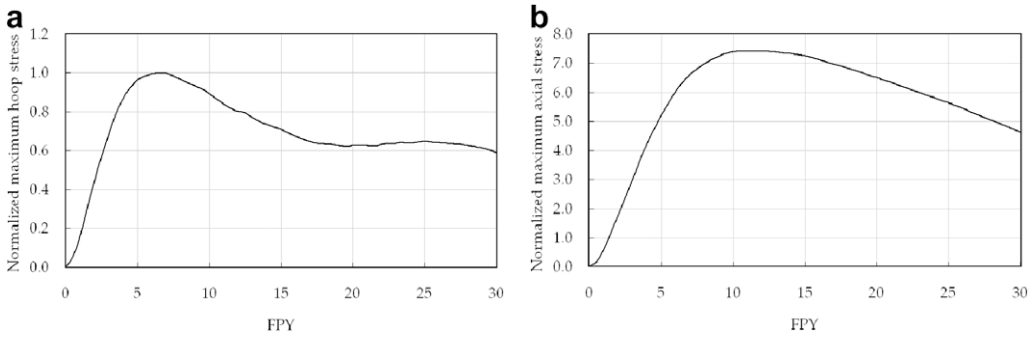

Fig. 7. Baseline solution for unmodified PGA graphite brick: (a) normalized maximum hoop stress; (b) normalized maximum axial stress.

Table 2
Summary of stress variations for sensitivity studies

Case	Varying material property	Results for peak hoop stress Change in property (%)				Results for peak axial stress Change in property (%)			
		20	10	+10	+20	20	10	+10	+20
Elastic strain study									
1	Young's modulus (perp.)	1.803	0.819	0.657	1.199	0.015	0.007	0.006	0.010
2	Young's modulus (para.)	0.453	0.202	0.166	0.304	1.328	0.620	0.531	0.964
3	Poisson's ratio (perp.)	0.057	0.029	0.029	0.057	0.000	0.000	0.000	0.000
4	Poisson's ratio (para.)	0.421	0.210	0.211	0.421	0.001	0.000	0.001	0.001
Creep strain study									
5	Creep modulus (perp.)	13.532	6.775	6.765	13.246	0.107	0.047	0.037	0.067
6	Creep modulus (para.)	2.566	1.181	1.236	2.555	19.040	9.454	9.349	18.600
7	Creep Poisson's ratio (perp.)	0.341	0.171	0.172	0.345	0.003	0.001	0.002	0.003
8	Creep Poisson's ratio (para.)	2.533	1.267	1.270	2.542	0.085	0.044	0.046	0.094
Dimensional change strain study									
9	Dimensional change (perp.)	8.844	4.460	4.460	8.920	0.032	0.016	0.016	0.032
10	Dimensional change (para.)	11.017	5.613	5.613	11.466	20.284	10.142	10.142	20.288
Thermal strain study									
11	CTE (perp.)	0.825	0.413	0.413	0.825	0.013	0.006	0.006	0.013
12	CTE (para.)	0.089	0.045	0.045	0.089	0.386	0.193	0.193	0.386

6.1. Elastic strain study

In this subsection only the elastic properties, i.e. Young's modulus and Poisson's ratio are varied in the perpendicular and parallel directions. All the others material properties remain unchanged (i.e. the creep modulus does not change with elastic modulus). Only one of the elastic properties is varied in each case by ±10% and ±20%. The results are summarized in Table 2. Despite significant changes to the elastic modulus the stresses vary little from the baseline solution. The reason for this is that the main driving force, dimensional change rate, is not modified and any change in stress associated with change in modulus is rapidly crept out. In addition the low values of Poisson's ratio, particularly in the parallel direction, gives only limited transverse coupling to any of small changes in elastic stress.

6.2. Creep strain study

In this subsection only the creep properties are considered. All the others material properties remain unchanged. Only one of the creep properties is varied in each case by ±10% and ±20%. The results are presented in Figs. 8–11 and also summarized in Table 2. In this case there are significant changes to the through life stresses in the direction in which the creep modulus is change. However, transverse to the modified modulus the change in stress is much less due to the low values of creep Poisson's ratio. Changing creep Poisson's ratio alone makes only a small change as can be seen from Figs. 10 and 11.

6.3. Dimensional change study

In this subsection only the dimensional change properties are varied in the perpendicular and parallel directions by ±10% and ±20%. The results are presented in Figs. 12 and 13 and summarized in Table 2. Dimensional change is the main driving force giving rise to the stresses. Modifying dimensional change significantly alters the stresses. The apparent low coupling between changes in perpendicular and parallel direction, as showed in Fig. 12 is probably a reflection of the large difference in stress in the two component directions.

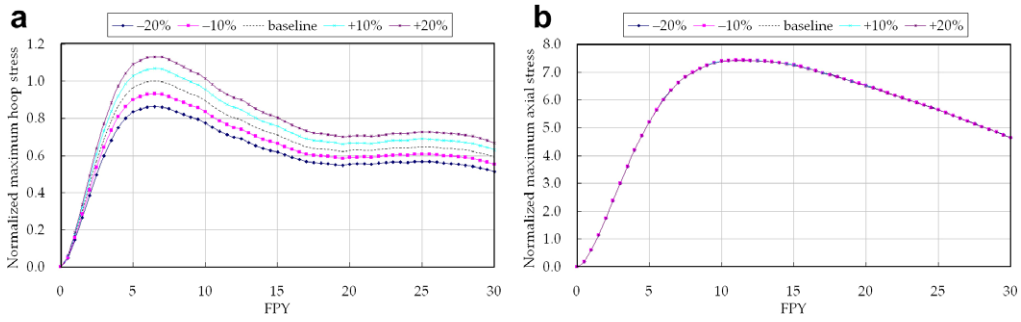

Fig. 8. Maximum stress results for varying of perpendicular creep modulus: (a) normalized maximum hoop stress; (b) normalized maximum axial stress.

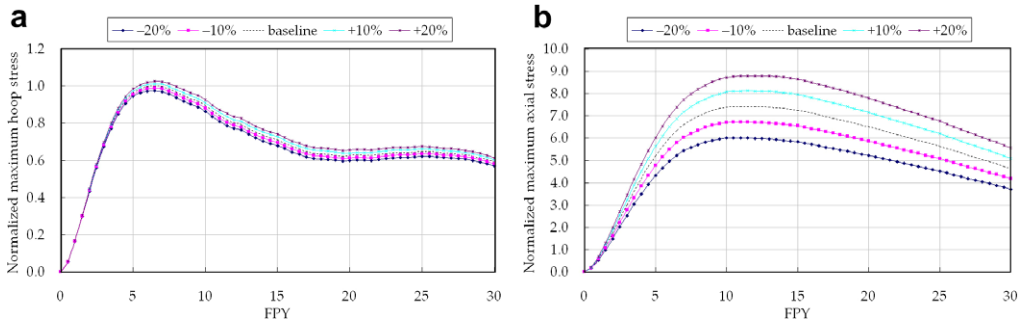

Fig. 9. Maximum stress results for varying of parallel creep modulus: (a) normalized maximum hoop stress; (b) normalized maximum axial stress.

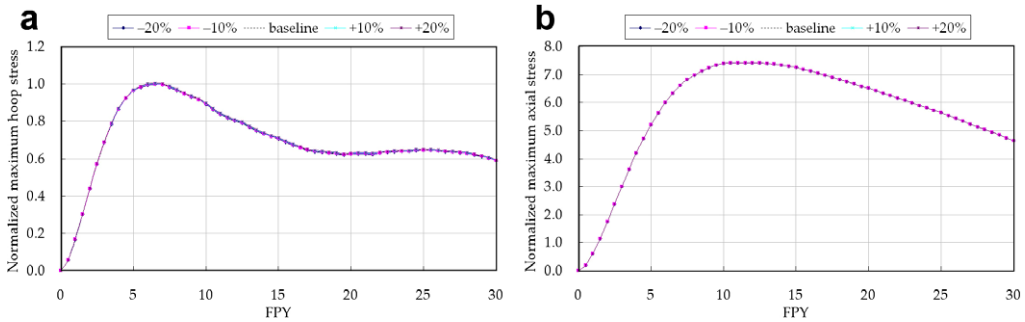

Fig. 10. Maximum stress results for varying of perpendicular creep Poisson's ratio: (a) normalized maximum hoop stress; (b) normalized maximum axial stress.

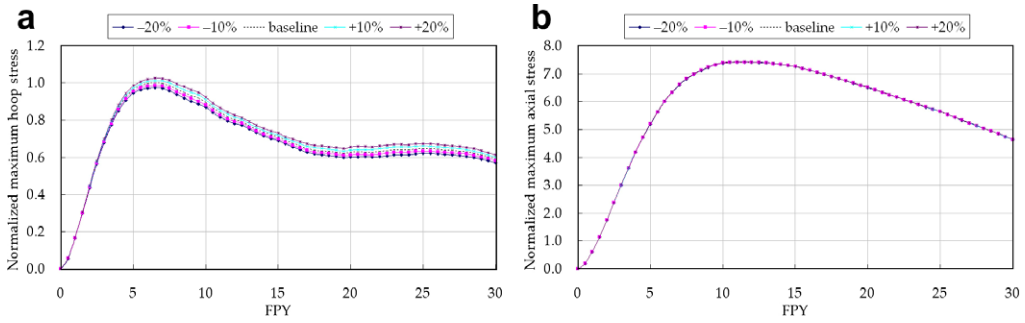

Fig. 11. Maximum stress results for varying of parallel creep Poisson's ratio: (a) normalized maximum hoop stress; (b) normalized maximum axial stress.

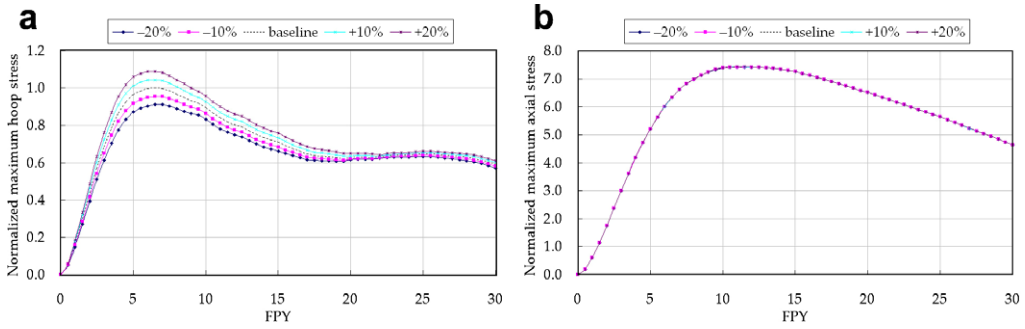

Fig. 12. Maximum stress results for varying of perpendicular dimensional change: (a) normalized maximum hoop stress; (b) normalized maximum axial stress.

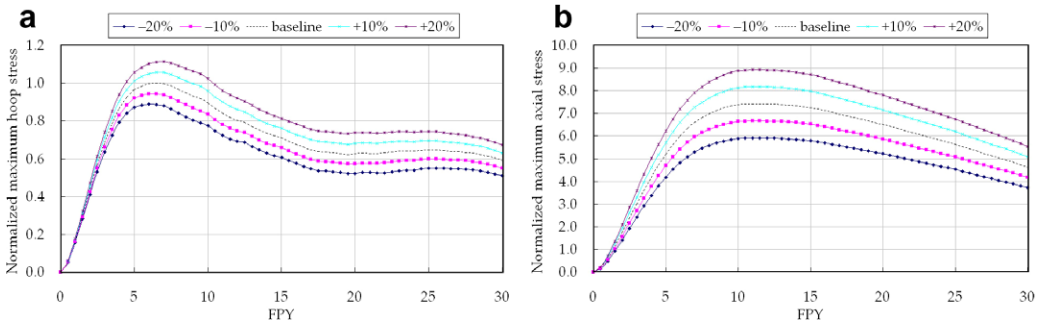

Fig. 13. Maximum stress results for varying of parallel dimensional change: (a) normalized maximum hoop stress; (b) normalized maximum axial stress.

6.4. Thermal strain study

In this subsection the effect of varying the coefficient of thermal expansion used to calculate thermal strain is studied. The irradiated values of CTE are varied in the perpendicular and parallel directions by ±10% and ±20%. The results are summarized in Table 2. Changes to the irradiated values of CTE make little difference. This is probably due to the low values of CTE in PGA graphite.

7. Conclusions

1. A constitutive model for predicting irradiation induced stresses in anisotropic graphite component components is presented. The model can account for damage due to fast neutron irradiation and radiolytic oxidation.
2. As an example of the use this model, stress analysis in a typical Magnox graphite moderator brick are presented. The brick is assumed to be manufactured from Pile Grade A (PGA) graphite.
3. A series of sensitivity studies on material input data are also presented. The results suggest that the variation in creep modulus and dimensional change have most significant effect on stress.

Acknowledgements

The authors would like to thank the UK Health and Safety Executive (Nuclear Safety Directorate) for financial support. The views expressed in this paper are those of the authors and do not necessarily represent those of the Health and Safety Executive.

References

[1] D.K.L. Tsang, B.J. Marsden, J. Nucl. Mater. 350 (2006) 208.
[2] ABAQUS, Hibbit, Karlsonn and Sorensen, 2006.
[3] J.E. Brocklehurst, B.T. Kelly, Carbon 31 (1993) 155.
[4] D.K.L. Tsang, B.J. Marsden, S.L. Fok, G. Hall, Carbon 43 (2005) 2902.
[5] B.T. Kelly, J.E. Brocklehurst, J. Nucl. Mater. 65 (1977) 79.